nature chemistry

ARTICLES

PUBLISHED ONLINE: 26 FEBRUARY 2012 | DOI: 10.1038/NCHEM.1277

Topological insulator nanostructures for near-infrared transparent flexible electrodes

Hailin Peng[1]*, Wenhui Dang[1], Jie Cao[1], Yulin Chen[2,3], Di Wu[1], Wenshan Zheng[1], Hui Li[1], Zhi-Xun Shen[3,4] and Zhongfan Liu[1]

Topological insulators are an intriguing class of materials with an insulating bulk state and gapless Dirac-type edge/surface states. Recent theoretical work predicts that few-layer topological insulators are promising candidates for broadband and high-performance optoelectronic devices due to their spin-momentum-locked massless Dirac edge/surface states, which are topologically protected against all time-reversal-invariant perturbations. Here, we present the first experimental demonstration of near-infrared transparent flexible electrodes based on few-layer topological-insulator Bi_2Se_3 nanostructures epitaxially grown on mica substrates by means of van der Waals epitaxy. The large, continuous, Bi_2Se_3-nanosheet transparent electrodes have single Dirac cone surface states, and exhibit sheet resistances as low as ~330 Ω per square, with a transparency of more than 70% over a wide range of wavelengths. Furthermore, Bi_2Se_3-nanosheet transparent electrodes show high chemical and thermal stabilities as well as excellent mechanical durability, which may lead to novel optoelectronic devices with unique properties.

Transparent conductive electrodes are an essential component of modern optoelectronics devices, including displays, organic light-emitting diodes (OLEDs), touch screens and solar cells[1]. Doped metallic oxides (mainly indium tin oxide, ITO) are predominantly used as the materials for such applications because of their high electrical conductivity, good optical transparency in the visible light region and unlimited scalability. However, the limited natural abundance of ITO, as well as the relatively high reflectivity, insufficient flexibility and limited near-infrared (NIR) transparency of ITO films, severely restrict its use in the next generation of optoelectronic devices. Transparent conductors with a high infrared transmittance are particularly attractive for applications in infrared imaging and sensing, infrared emission devices, modulators and switches for fibre-optic communications, and NIR-sensitive solar cells[1]. Emerging nanomaterials such as carbon nanotubes[2,3], graphene[4,5], metallic nanowires[6–8] and printable metal grids[9] are currently believed to be the leading alternatives or complements to ITO. Other novel transparent conductive materials with unique properties remain highly desirable.

Layered bismuth selenide (Bi_2Se_3), an important narrow-bandgap semiconductor for high-performance infrared detectors and thermoelectric applications[10], has recently been demonstrated to be a reference three-dimensional topological insulator[11–15] with a large insulating bulk gap of ~0.3 eV and metallic surface states consisting of a single Dirac cone[16–18]. A new type of two-dimensional electron gas (2DEG) covers the whole surface of Bi_2Se_3 where the electron spins are locked to their linear momentum[16]. The helical nature of the surface state suppresses electron backscattering and can enable excellent transport properties with a high carrier mobility of ~6,000 $cm^2\ V^{-1}\ s^{-1}$ and a Fermi velocity of ~5×10^5 $m\ s^{-1}$ (refs 16,19). Furthermore, surface conduction can be significantly enhanced and easily manipulated in few-layer topological-insulator nanostructures with large surface-to-volume ratios[20–23]. For example, pronounced Aharonov–Bohm oscillations were recently observed in Bi_2Se_3 nanoribbons[20], the first example of quantum interference associated with non-trivial surface states of topological insulators.

The single-Dirac-cone surface state of Bi_2Se_3 can be imagined as 1/4 graphene in which spin and valley degrees of freedom result in four Dirac cones. In analogy to the optoelectronics applications of graphene, a thin layer of topological insulator has been theoretically predicted to be a promising material for broadband and high-performance optoelectronic devices such as photodetectors, terahertz lasers, waveguides and transparent electrodes[24]. Topologically protected and spin-momentum-locked massless Dirac-type surface states are key features of topological insulators and provide many new opportunities for enhancing the performance of these materials for optoelectronics applications. Here, we present the first experimental realization of transparent flexible electrodes based on topological-insulator Bi_2Se_3 nanostructures. Large-area, few-layer Bi_2Se_3 nanosheets of variable thickness were epitaxially grown on a fluorophlogopite mica substrate by means of van der Waals epitaxy. The robust surface states consisting of a single Dirac cone at the Γ point were observed in as-grown Bi_2Se_3 nanosheets by angle-resolved photoemission spectroscopy (ARPES) measurements. Bi_2Se_3 nanosheets with a thickness of ~10 nm exhibit a low sheet resistance of 330 Ω $\square^{-1}$, which is comparable to that of graphene synthesized by chemical vapour deposition (~275 Ω $\square^{-1}$)[5], and a transparency of more than 70% in the 1,000–3,000 nm wavelength regime. Unlike single-layer graphene films, the conductivities of Bi_2Se_3 nanosheets are quite resistant to oxygen plasma treatment. Furthermore, transparent electrodes based on Bi_2Se_3 nanosheets are durable over 1,000 bending cycles, showing excellent mechanical flexibility.

Results and discussion

Layered Bi_2Se_3 has a rhombohedral crystal structure in the space group D_{3d}^5 ($R\bar{3}m$), with each quintuple layer consisting

[1]Center for Nanochemistry, Beijing National Laboratory for Molecular Sciences (BNLMS), State Key Laboratory for Structural Chemistry of Unstable and Stable Species, College of Chemistry and Molecular Engineering, Peking University, Beijing 100871, PR China, [2]Department of Physics and Clarendon Laboratory, University of Oxford, Parks Road, Oxford, OX1 3PU, UK, [3]Stanford Institute for Materials and Energy Sciences, SLAC National Accelerator Laboratory, 2575 Sand Hill Road, Menlo Park, California 94025, USA, [4]Geballe Laboratory for Advanced Materials, Departments of Physics and Applied Physics, Stanford University, Stanford, California 94305, USA. *e-mail: hlpeng@pku.edu.cn

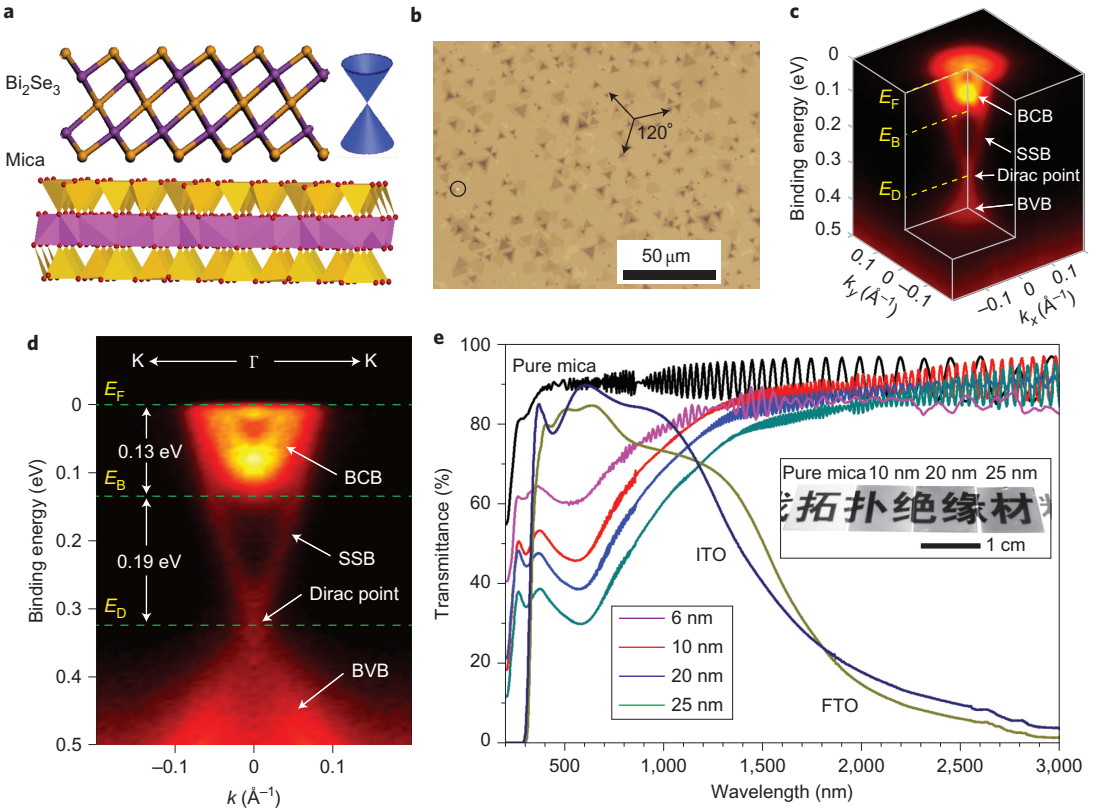

Figure 1 | Synthesis and spectroscopy characterization of the Bi_2Se_3 nanosheets on thin mica sheet substrates. a, Schematic diagram of few-layer Bi_2Se_3 nanosheets epitaxially grown on a thin sheet of fluorophlogopite mica. The cones of the Bi_2Se_3 surface illustrate the Dirac surface states with linear dispersion. **b**, Typical optical microscopy image in transmission mode of large-area, few-layer Bi_2Se_3 nanosheets grown on a mica substrate. The blank mica substrate is indicated by the black circle. **c**, Three-dimensional illustration of the electronic band structure from ~10-nm-thick Bi_2Se_3 nanosheets grown on a mica substrate measured by ARPES, showing a single surface Dirac cone at the centre of the Brillouin zone. The BCB, BVB and SSB are indicated, together with the Fermi energy (E_F), the bottom of the BCB (E_B) and the Dirac point (E_D). **d**, ARPES band dispersion along the K-Γ-K direction of the Bi_2Se_3 nanosheets. The BCB bottom is ~130 meV below E_F and ~190 meV above E_D. **e**, UV-vis-IR spectra of Bi_2Se_3 nanosheets of different thicknesses on mica, as well as for pure mica substrate (black), ITO (blue) and FTO (olive). The sharp oscillatory features are Fabry–Perot interference effects, identified due to internal reflections in the atomically layered structures of mica and Bi_2Se_3. Inset: photograph of Bi_2Se_3 nanosheets of various thicknesses on mica and of a pure mica substrate, showing their good visible transparency.

of Se–Bi–Se–Bi–Se sheets[25]. The planar, covalently bonded quintuple layers are held together by weak van der Waals interactions (Fig. 1a). The van der Waals epitaxial growth of large-area, few-layer Bi_2Se_3 nanosheets used in the present work was achieved using a set-up similar to our previous nanoribbon and nanoplate synthesis[20,26]. The property of the growth substrate is important for controlling the morphology and thickness of the Bi_2Se_3 products. One excellent substrate for van der Waals epitaxy of Bi_2Se_3, fluorophlogopite mica [$KMg_3(AlSi_3O_{10})F_2$], has a two-dimensional sheet structure with pseudohexagonal Z_2O_5 sheets (Z = Si and Al) formed by ZO_4 tetrahedrons. Notably, fluorophlogopite mica can be perfectly cleaved into few-micrometre-thick sheets, which are atomically smooth, chemically inert, thermally stable, highly transparent, flexible and perfectly insulating (Supplementary Fig. S1). These outstanding properties make fluorophlogopite mica a favourable substrate for the direct growth and optical and electrical measurements of Bi_2Se_3 nanosheets in topological-insulator-based transparent flexible electrodes.

As-grown Bi_2Se_3 nanosheet films were first characterized using optical microscopy. Figure 1b shows a typical optical microscopy image in transmission mode of a large continuous Bi_2Se_3 nanosheet film on a transparent fluorophlogopite mica substrate. Small triangular or hexagonal nanoplate islands were formed on the uniform nanosheet with identical orientations, suggesting the epitaxial growth nature of the Bi_2Se_3 nanostructures. Such a nanosheet film begins as Bi_2Se_3 nuclei at random locations on the mica and, as growth continues, these nuclei epitaxially grow into oriented nanoplate arrays and eventually coalesce to form an interconnected nanosheet film. Nanosheet films with tunable thickness were obtained by varying the growth time and deposition temperature. The thickness and surface roughness of as-grown nanosheets can be roughly identified from the difference in contrast seen in the optical microscopy images and further determined by atomic force microscopy (AFM; Supplementary Fig. S2).

We used ARPES to investigate the electronic band structures of ~10-nm-thick Bi_2Se_3 nanosheets grown on mica. Our ARPES measurements unambiguously identified the existences of both a direct bulk gap and a single-Dirac-cone surface state (Fig. 1c,d), hallmarks of the topological insulator Bi_2Se_3 (refs 17,27). A Dirac point, the apex of the V-shaped dispersion of the surface state band (SSB), is located at ~320 meV below the Fermi level (E_F) and ~190 meV below the bottom of the bulk conduction band (BCB). A sharp rim emerges around the BCB bottom, which is assigned to a quantum-confined 2DEG near the surface. The lower part of the Dirac cone is broadened due to hybridization with the bulk valence band (BVB)[17,27]. Note that although the BCB appears partially occupied due to the n-type doping from defects during growth and ambient doping[17,27], the Dirac cone of the surface state can still be clearly seen in months-old samples that have been exposed to air for a few days. This observation

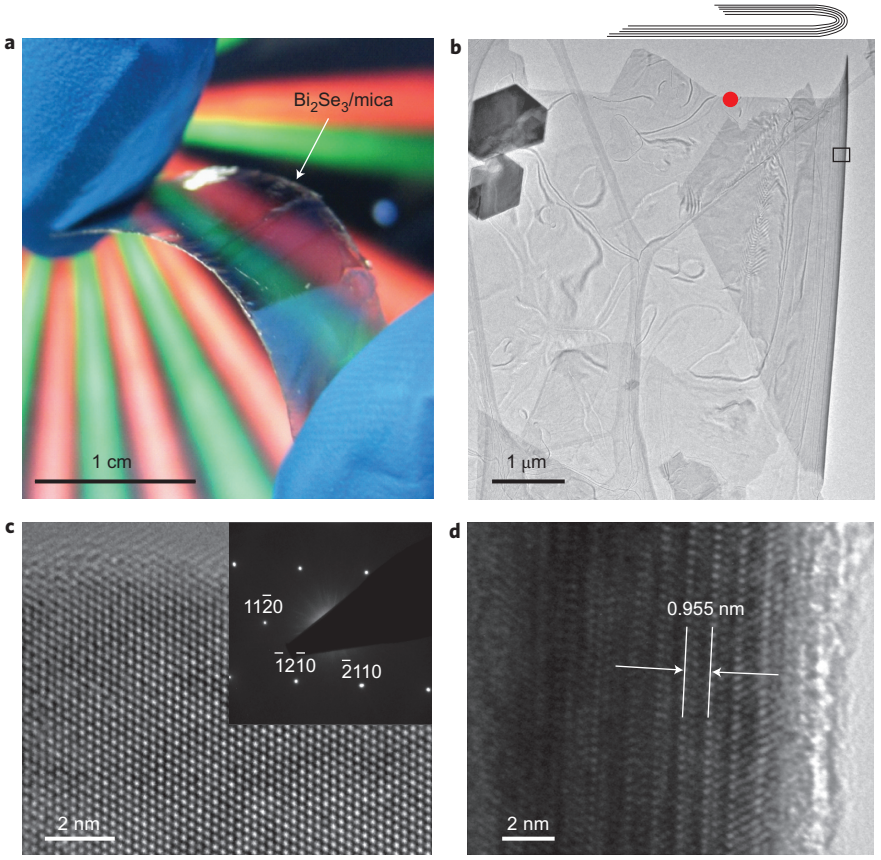

Figure 2 | Structure characterization of the flexible Bi_2Se_3 nanosheets. a, Photograph of a transparent thin Bi_2Se_3/mica flake, demonstrating its flexibility. **b**, Bright-field TEM image of a free-standing Bi_2Se_3 film with a folded edge. **c**, HRTEM image of the red spot in **b**, showing the highly crystalline nature of the basal plane of the as-grown Bi_2Se_3 film. Inset: corresponding normal incident SAED pattern of the Bi_2Se_3 film. **d**, HRTEM image of the folded edge of the Bi_2Se_3 film showing layered structures with periodical fringes corresponding to layer number. Recording position indicated by the black square in **b**.

confirms the robust nature of the topological surface states of Bi_2Se_3 nanosheets. From ARPES measurements, we can estimate that the number of carriers from surface states at the top and bottom surfaces is about the same as that for bulk bands for such a 10-nm-thick sample (Supplementary Fig. S3), confirming the non-negligible contribution from surface states to the total conductivity because of the large surface-to-volume ratio of these nanosheets.

The transparency of as-grown topological-insulator Bi_2Se_3 nanosheet films was evaluated using ultraviolet-visible-infrared (UV–vis–IR) spectroscopy. As shown in Fig. 1e, UV–vis–IR spectra reveal that the optical transmittance of the Bi_2Se_3 nanosheet films depends on the film thickness. Note that fluorophlogopite mica exhibits extraordinary transmittance in the UV–vis–IR regime (0.25–4.5 μm) without any sharp absorption features. On this transparent mica substrate, a ~6-nm-thick Bi_2Se_3 nanosheet film with a roughness of ~1 nm has an average visible transmittance between 60 and 70%. Although this result is not better than that for conventional ITO, the ultrathin Bi_2Se_3 film has a total transmittance of more than 80% in the wavelength range 1–3 μm, which is comparable to that of graphene films. Most noticeably, in the short-wavelength infrared region (1.4–3 μm), in contrast to ITO glass ($20\ \Omega\ \square^{-1}$, from BBMA) and fluorine tin oxide (FTO glass, from NSG, 2.2 mm in thickness, $14\ \Omega\ \square^{-1}$), which become optically opaque due to free-electron plasma resonance, the Bi_2Se_3 nanosheet films demonstrate an outstanding transmittance of ~90%. The high infrared transmittance (or low absorption), particularly in the NIR region, is mainly due to the free-carrier plasma edge located in the far-infrared frequency[28]. The direct photoexcitation of carriers within the surface state of a topological insulator is forbidden due to the non-spin degeneracy, which may give rise to high optical transmission in the infrared region. These unique optical properties make the topological-insulator Bi_2Se_3 nanosheet a promising candidate for use in window electrodes for displays, solar cells, pyroelectric detectors and OLEDs over a wide range of wavelengths.

As well as their high transparency, Bi_2Se_3 nanosheets on mica substrates exhibit outstanding structural integrity and flexibility (Fig. 2a). Thin films of inorganic materials exhibit remarkable flexibility because bending strains are directly proportional to thickness[29]. The layered structure of Bi_2Se_3 is ideal for achieving ultrathin films with high crystalline quality. We found that thin Bi_2Se_3 nanoribbons and nanosheets can be easily bent to $>180^\circ$ with a radius of less than 10 μm without breaking, which suggests that ultrathin nanoribbons and nanosheets are rather flexible in contrast to the fragile bulk crystal of Bi_2Se_3 (Supplementary Figs S4 and S5). Transmission electron microscopy (TEM) was used to examine the microstructure and mechanical flexibility of the Bi_2Se_3 nanosheets. Free-standing Bi_2Se_3 nanosheets were transferred from the mica substrate to a lacey carbon support film on a TEM grid with the assistance of a drop of dilute HF solution (2% v/v). Figure 2b shows a typical TEM image of a Bi_2Se_3 nanosheet with a folded edge. The high-resolution TEM (HRTEM) image in Fig. 2c shows the expected hexagonal lattice fringes with a lattice spacing of 0.21 nm, consistent with the spacing of the (11–20) planes of layered Bi_2Se_3. A corresponding selected area electron diffraction (SAED) image confirmed the single crystalline nature of the Bi_2Se_3 nanosheet. Energy-dispersive X-ray spectroscopy (EDX) analysis of the nanosheet indicated a bismuth/selenium atomic ratio of ~2/3, within the accuracy of the measurements

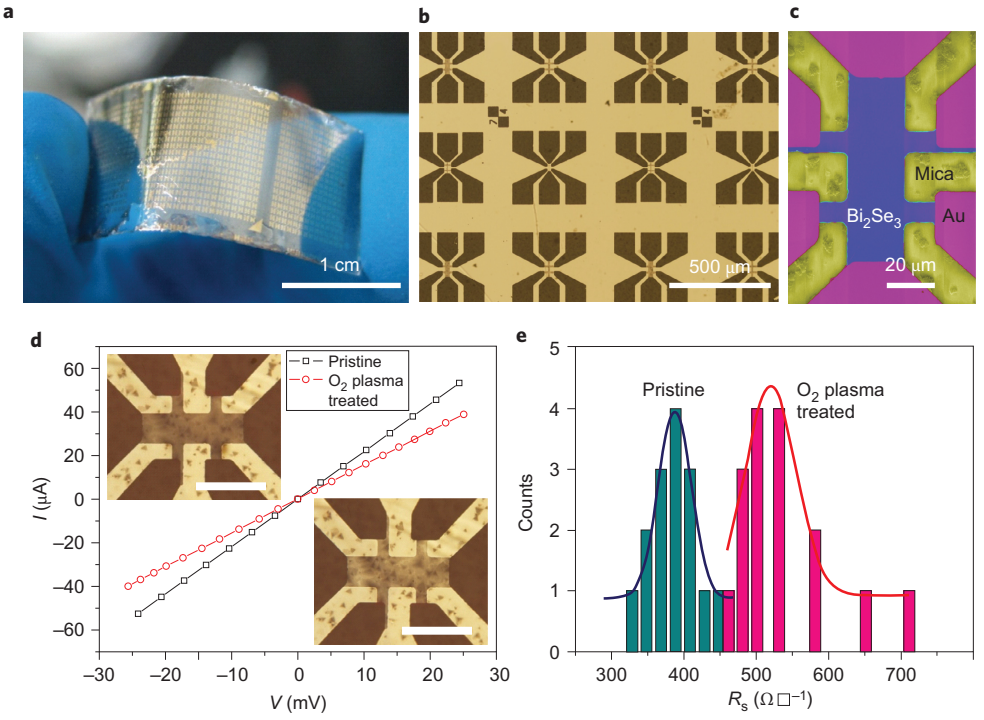

Figure 3 | Electrical characterization of Bi_2Se_3 nanosheets on mica substrates. a, Photograph of a patterned Hall bar array composed of an ~10-nm-thick Bi_2Se_3 nanosheet on a transparent mica substrate. **b**, Transmission-mode optical microscopy image of the Bi_2Se_3 Hall bar array. **c**, SEM image (false colour) of an individual Bi_2Se_3 Hall bar structure (blue) on a mica substrate (yellow) contacted by chromium/gold electrodes (purple). **d**, Typical electrical measurement for the Bi_2Se_3 nanosheet before and after 20 s oxygen plasma treatment. Insets on the left and right are optical microscopy images of the same device before and after oxygen plasma treatment, respectively. **e**, Histogram of sheet resistance distribution of Bi_2Se_3 nanosheets before and after oxygen plasma treatment for 15 active devices.

(Supplementary Fig. S6). The structural integrity and uniformity of the nanosheets were also confirmed by micro-Raman spectroscopy and two-dimensional mapping (Supplementary Fig. S7). The HRTEM image of the folded edge of the nanosheet reveals that the nanosheet (thickness, ~10 nm) can be bent to 180° without any fractures (Fig. 2d). Inside the folding region, the Bi_2Se_3 nanosheet exhibits an expected moiré pattern, characteristic of rotation-mismatched multilayer films.

For the macroscopic conductive electrode application, the electrical transport properties of the Bi_2Se_3 nanosheets were measured using four-point-contact devices on patterned Hall bar structures. The use of dielectric mica substrates is compatible with device fabrication procedures, which facilitates the transfer-free batch fabrication of Bi_2Se_3 nanosheet devices. Thus, potential damage during the nanosheet transfer process is avoided. We used standard photolithography to directly fabricate arrays of Hall bar devices of as-grown Bi_2Se_3 nanosheets with various channel widths, the smallest being 2 μm. A representative photograph and optical image of the Hall bar array are shown in Fig. 3a,b, with chromium/gold (5 nm/50 nm) deposited on the insulating mica substrate as the contact metal. From the scanning electron microscopy (SEM) image of an individual Hall bar device, the channel length and width were determined to be 75 and 20 μm, respectively (Fig. 3c). The source–drain current versus voltage characteristic of a pristine Bi_2Se_3 nanosheet (Fig. 3d) is linear and symmetric, with a four-probe resistance of 475 Ω and a sheet resistance of 360 Ω □$^{-1}$. The measured contact resistance is ~30 Ω per contact, much less than the channel resistance. Measurements of 10-nm-thick Bi_2Se_3 nanosheet devices with various channel widths reveal that the lowest sheet resistance is 330 Ω □$^{-1}$ and average sheet resistance remains 390 Ω □$^{-1}$ (Fig. 3e).

The durability of the transparent electrodes against elevated temperature, high humidity and strong chemical agents in the ambient environment has widespread importance for practical applications. The non-trivial surface states of topological-insulator Bi_2Se_3 are robust, and the topological protection makes the conductive electrodes highly resistant to the ambient environment. Indeed, the Bi_2Se_3 nanosheet films remained intact and exhibited good conductivity after heating to as high as 300 °C. Furthermore, the conductivity of Bi_2Se_3 nanosheet films changed little under a wide range of relative humidity (2–80%; Supplementary Fig. S8). To further verify the robustness of the Bi_2Se_3 conductive electrodes, we carried out an oxygen plasma treatment of the Bi_2Se_3 nanosheet devices. The Bi_2Se_3 nanosheets on mica substrates were directly exposed to a plasma mixture of oxygen/nitrogen gas (1:4) (Prep2-FEMTO, Diener Electronic) under an input power of 90 W for a few seconds. After plasma treatment, the Bi_2Se_3 nanosheet became more transparent (Fig. 3d, insets), suggesting the formation of the electrically insulating oxide layer on the top surface of the film. Surprisingly, the I–V curve for the plasma-treated Bi_2Se_3 nanosheet remained linear with a resistance of 640 Ω, slightly higher than the 475 Ω of the initial Bi_2Se_3 nanosheet (Fig. 3d). Unlike single-layer transparent graphene electrodes, which are easily destroyed during oxygen plasma treatment, the resistance statistics for plasma-treated Bi_2Se_3 devices show an average sheet resistance of ~520 Ω □$^{-1}$ (Fig. 3e). The resistance distribution becomes wider, presumably due to variations in the thickness and surface roughness of the plasma-treated films. As well as inducing structural disorder, the oxygen plasma treatment may also create chemical functional groups such as OH, Bi–O, Se–O, and so on, which can lead to chemical doping in the Bi_2Se_3 nanosheets. In fact, most naturally grown Bi_2Se_3 nanostructures are n-type doped in bulk due to selenium vacancies and further n-type doped after exposure to air[30], as confirmed by our ARPES measurements. In doped Bi_2Se_3 nanosheets, the total conductance predominantly occurs through

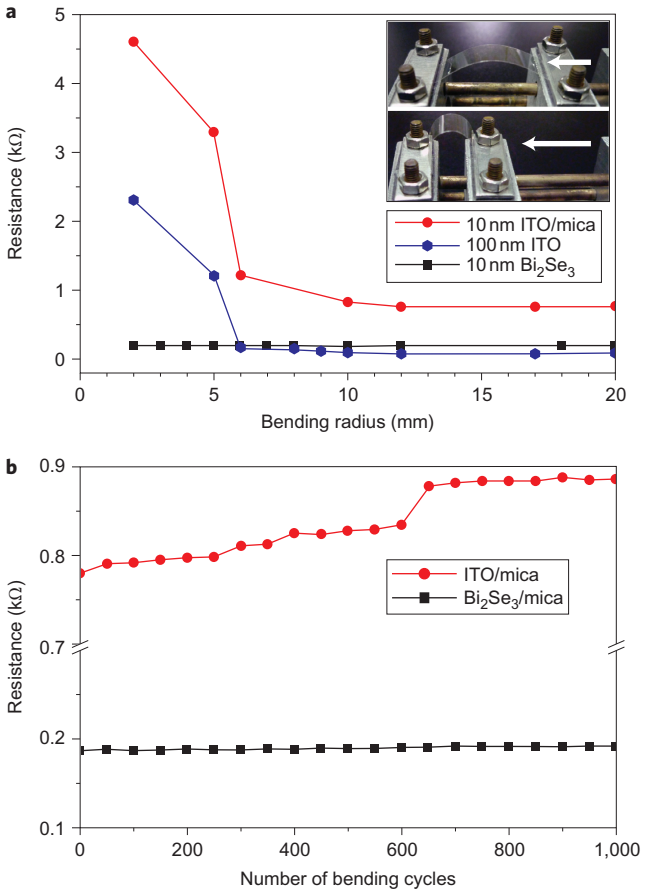

Figure 4 | Durability of the Bi_2Se_3 transparent electrode. a, Resistance change of a ~10-nm-thick Bi_2Se_3 sheet film on a 0.05-mm-thick mica substrate compared with sputtered ITO/mica electrodes for different bending radii. Inset: bending process. **b**, Resistance change in response to cycles of bending (to a 10 mm radius) of the 10-nm-thick Bi_2Se_3 sheet on mica compared with 10-nm-thick ITO on mica.

the top and bottom surface-state channels as well as the doped bulk channel[22]. Even when the very top surface is degraded by contamination and disorder, the Dirac surface state remains, which, together with the bottom surface state and predominant parallel bulk conduction, enables the nanosheet to remain highly conductive.

Mechanical durability is another important feature for the transparent electrodes used in the next generation of optoelectronic devices. A lack of flexibility and inherent fragility severely limit the use of traditional ITO thin films. In contrast, topological-insulator Bi_2Se_3 nanostructures exhibit significant structural flexibility in addition to their unique optical and electrical properties. We evaluated the durability of the topological-insulator Bi_2Se_3 transparent electrodes by measuring resistance with respect to bending radius. Figure 4a plots the results of resistance tests on a Bi_2Se_3 nanosheet film grown on a mica flake as a function of different bending radii (Supplementary Fig. S9). Unlike sputtered ITO/mica thin-film electrodes, which easily degrade with a bending radius of less than ~6 mm, the ~10-nm-thick Bi_2Se_3 nanosheets grown on mica kept their structural integrity, with little variation in resistance, up to a bending radius of 2 mm, which is comparable to the results for graphene films[5]. The bending radius is not limited by the Bi_2Se_3 nanosheet itself, but by the mica substrate and coated chromium/gold contacts. Given a more flexible substrate, the Bi_2Se_3 conductive electrode might exhibit durability to an even smaller bending radius as a result of its ultrathin thickness and high crystalline quality. Note that the Bi_2Se_3 nanosheet can recover its original resistance after repeated dynamic bending tests, in contrast to sputtered ITO films. The resistance of the Bi_2Se_3 electrode increased only ~3% after 1,000 bending cycles (Fig. 4b), indicating its excellent durability. It is theoretically predicted that the topological surface states are protected by time-reversal symmetry and are immune to localization, therefore remaining conductive under a high density of defects and dislocations[31]. The robust topological surface states may preserve the electrical conduction of the Bi_2Se_3 film under large strain or other distortions during mechanical bending, further improving its performance as a flexible transparent electrode.

Conclusions

We have developed a simple method to directly grow large-area, transparent, flexible topological-insulator Bi_2Se_3 nanosheets on mica substrates by means of van der Waals epitaxy. The few-layer topological-insulator nanosheets show promise as transparent flexible electrodes because of their superior near-infrared transparency and excellent conductivity, which is robust against surface contaimination and bending. The unique optical, electrical and mechanical properties of the topological-insulator Bi_2Se_3 nanosheet films enable the production of exotic transparent flexible electrodes, paving the way for future nanoelectronics, photoelectronics and other novel applications.

Methods

Bi_2Se_3 nanosheet growth. Bi_2Se_3 nanosheets were grown inside a 12-inch horizontal tube furnace (Lindberg/Blue M) equipped with a 1-inch-diameter quartz tube. Bi_2Se_3 powder (Alfa Aesar, purity 99.999%) was placed in the hot centre of the tube furnace as the source material for evaporation. Argon was used as the carrier gas to transport the vapour to the colder furnace region. The freshly cleaved fluorophlogopite mica substrates (thickness, ~20–80 μm) were placed downstream at certain locations with accurately set temperatures. The tube was pumped to a base pressure of 50 mtorr and flushed with the carrier gas repeatedly to decrease oxygen contamination. Typical growth conditions were a source temperature of 500 °C, pressure of 100 torr, carrier gas flow rate of 500 s.c.c.m., growth temperature of 290–390 °C and growth time of 5–30 min.

Device fabrication. The use of dielectric mica substrates is compatible with device fabrication procedures, facilitating the transfer-free batch fabrication of Bi_2Se_3 nanosheet Hall bar devices. Standard photolithography was used to define the selected region and fabricate arrays of Hall bar devices of as-grown Bi_2Se_3 nanosheets. Plasma etching (50 W, 30 Pa) was used to remove the unwanted nanosheet regions and finalize the Hall bar structures. Thermal evaporation was performed to deposit the metal electrodes, with chromium/gold (5 nm/50 nm) as the contacts, which were found to form ohmic contact without annealing.

Characterization. Characterization was carried out using optical microscopy (Olympus DX51 microscope), UV–vis–IR (Perkin Elmer Lambda 950 spectrophotometer), AFM (Vecco Nanoscope IIIa), SEM (Hitachi S-4800; acceleration voltage, 5–30 kV) and TEM (FEI Tecnai F30; acceleration voltage, 300 kV). A lacey carbon film supported on copper grids was used for TEM characterization. ARPES measurements were performed at 5–4 of the Stanford Synchrotron Radiation Lightsource (SSRL). The measurement pressure was kept at $<3 \times 10^{-11}$ torr, and data were recorded by Scienta R4000 analysers at a sample temperature of 10 K. The total convolved energy and angle resolutions were 10 meV and 0.2° (<0.007(1/Å) for photoelectrons generated by 21 eV photons). To avoid charging effects, samples were partially covered with patterned gold films. Before measurements, samples were heated to 150 °C to outgas adsorbed contaminations on the surface. Electrical measurements were carried out in a Micromanipulator 6200 probe station with a Keithley 4200 semiconductor analyser.

Received 15 September 2011; accepted 20 January 2012; published online 26 February 2012

References

1. Hecht, D. S., Hu, L. & Irvin, G. Emerging transparent electrodes based on thin films of carbon nanotubes, graphene, and metallic nanostructures. *Adv. Mater.* **23,** 1482–1513 (2011).
2. Zhang, D. *et al.* Transparent, conductive, and flexible carbon nanotube films and their application in organic light-emitting diodes. *Nano Lett.* **6,** 1880–1886 (2006).
3. Hu, L., Hecht, D. S. & Gruner, G. Percolation in transparent and conducting carbon nanotube networks. *Nano Lett.* **4,** 2513–2517 (2004).

4. Wang, X., Zhi, L. & Muellen, K. Transparent, conductive graphene electrodes for dye-sensitized solar cells. *Nano Lett.* **8,** 323–327 (2008).
5. Bae, S. *et al.* Roll-to-roll production of 30-inch graphene films for transparent electrodes. *Nature Nanotech.* **5,** 574–578 (2010).
6. Ju, S. *et al.* Fabrication of fully transparent nanowire transistors for transparent and flexible electronics. *Nature Nanotech.* **2,** 378–384 (2007).
7. Lee, J. Y., Connor, S. T., Cui, Y. & Peumans, P. Solution-processed metal nanowire mesh transparent electrodes. *Nano Lett.* **8,** 689–692 (2008).
8. Wu, H. *et al.* Low reflectivity and high flexibility of tin-doped indium oxide nanofiber transparent electrodes. *J. Am. Chem. Soc.* **133,** 27–29 (2011).
9. Kang, M. G. & Guo, L. J. Nanoimprinted semitransparent metal electrodes and their application in organic light-emitting diodes. *Adv. Mater.* **19,** 1391–1396 (2007).
10. Mishra, S. K., Satpathy, S. & Jepsen, O. Electronic structure and thermoelectric properties of bismuth telluride and bismuth selenide. *J. Phys. Condens. Matter* **9,** 461–470 (1997).
11. Bernevig, B. A., Hughes, T. L. & Zhang, S. C. Quantum spin Hall effect and topological phase transition in HgTe quantum wells. *Science* **314,** 1757–1761 (2006).
12. Kane, C. L. & Mele, E. J. Quantum spin Hall effect in graphene. *Phys. Rev. Lett.* **95,** 226801 (2005).
13. Fu, L., Kane, C. L. & Mele, E. J. Topological insulators in three dimensions. *Phys. Rev. Lett.* **98,** 106803 (2007).
14. Moore, J. E. & Balents, L. Topological invariants of time-reversal-invariant band structures. *Phys. Rev. B* **75,** 121306 (2007).
15. Qi, X. L., Hughes, T. L. & Zhang, S. C. Topological field theory of time-reversal invariant insulators. *Phys. Rev. B* **78,** 195424 (2008).
16. Zhang, H. *et al.* Topological insulators in Bi_2Se_3, Bi_2Te_3 and Sb_2Te_3 with a single Dirac cone on the surface. *Nature Phys.* **5,** 438–442 (2009).
17. Xia, Y. *et al.* Observation of a large-gap topological-insulator class with a single Dirac cone on the surface. *Nature Phys.* **5,** 398–402 (2009).
18. Zhang, Y. *et al.* Crossover of the three-dimensional topological insulator Bi_2Se_3 to the two-dimensional limit. *Nature Phys.* **6,** 584–588 (2010).
19. Kou, X. F. *et al.* Epitaxial growth of high mobility Bi_2Se_3 thin films on CdS. *Appl. Phys. Lett.* **98,** 242102 (2011).
20. Peng, H. *et al.* Aharonov–Bohm interference in topological insulator nanoribbons. *Nature Mater.* **9,** 225–229 (2010).
21. Xiu, F. *et al.* Manipulating surface states in topological insulator nanoribbons. *Nature Nanotech.* **6,** 216–221 (2011).
22. Steinberg, H., Gardner, D. R., Lee, Y. S. & Jarillo-Herrero, P. Surface state transport and ambipolar electric field effect in Bi_2Se_3 nanodevices. *Nano Lett.* **10,** 5032–5036 (2010).
23. Teweldebrhan, D., Goyal, V. & Balandin, A. A. Exfoliation and characterization of bismuth telluride atomic quintuples and quasi-two-dimensional crystals. *Nano Lett.* **10,** 1209–1218 (2010).
24. Zhang, X., Wang, J. & Zhang, S.-C. Topological insulators for high-performance terahertz to infrared applications. *Phys. Rev. B* **82,** 245107 (2011).
25. Wyckoff, R. W. G. *Crystal Structures* (Krieger, 1986).
26. Dang, W., Peng, H., Li, H., Wang, P. & Liu, Z. Epitaxial heterostructures of ultrathin topological insulator nanoplate and graphene. *Nano Lett.* **10,** 2870–2876 (2010).
27. Chen, Y. L. *et al.* Massive Dirac fermion on the surface of a magnetically doped topological insulator. *Science* **329,** 659–662 (2010).
28. LaForge, A. D. *et al.* Optical characterization of Bi_2Se_3 in a magnetic field: infrared evidence for magnetoelectric coupling in a topological insulator material. *Phys. Rev. B* **81,** 125120 (2010).
29. Rogers, J. A., Lagally, M. G. & Nuzzo, R. G. Synthesis, assembly and applications of semiconductor nanomembranes. *Nature* **477,** 45–53 (2011).
30. Kong, D. *et al.* Rapid surface oxidation as a source of surface degradation factor for Bi_2Se_3. *ACS Nano* **5,** 4698–4703 (2011).
31. Nomura, K., Koshino, M. & Ryu, S. Topological delocalization of two-dimensional massless Dirac fermions. *Phys. Rev. Lett.* **99,** 146806 (2007).

Acknowledgements

The authors thank A. Y. Liu, D. S. Kong and X. L. Qi for helpful discussion. Thanks go to Q. Meng and Y. Gong for technical support with ITO sputtering. This work was financially supported by the National Science Foundation of China (nos 20973007, 20973013, 50821061, 21173004 and 11104003), the National Basic Research Program of China (nos 2012CB933404 and 2011CB921904). This work was financially sponsored by the Program for New Century Excellent Talents in universities (NCET) and the Scientific Research Foundation for Returned Overseas Chinese Scholars, the State Education Ministry (SRF for ROCS, SEM). Y.L.C. and Z.X.S. acknowledge support from the Department of Energy, Office of Basic Energy Sciences (contract no. DE-AC02-76SF00515).

Author contributions

H.P. conceived and designed the experiments. H.P., W.D. and D.W. performed the synthesis, structural characterization, device fabrication, transport measurements and analyses. Y.L.C. preformed the ARPES measurements. J.C., D.W., W.Z. and H.L. assisted in experimental work. H.P. wrote the paper. H.P. and Z.F.L. supervised the project and finalized the manuscript. All authors discussed the results and commented on the manuscript.

Additional information

The authors declare no competing financial interests. Supplementary information accompanies this paper at www.nature.com/naturechemistry. Reprints and permission information is available online at http://www.nature.com/reprints. Correspondence and requests for materials should be addressed to H.P.